

ARTICLES

Study of source size in $p\bar{p}$ collisions at $\sqrt{s} = 1.8$ TeV using pion interferometry

T. Alexopoulos,⁷ C. Allen,^{6,*} E. W. Anderson,⁴ V. Balamurali,⁵ S. Banerjee,^{5,†} P. D. Beery,^{5,‡} P. Bhat,³ J. M. Bishop,⁵ N. N. Biswas,⁵ A. Bujak,⁶ D. D. Carmony,⁶ T. Carter,^{2,†} Y. Choi,⁶ P. Cole,^{6,§} R. DeBonte,⁶ V. DeCarlo,¹ A. R. Erwin,⁷ C. Findeisen,^{7,||} A. T. Goshaw,² L. J. Gutay,⁶ A. S. Hirsch,⁶ C. Hojvat,³ J. R. Jennings,⁷ V. P. Kenney,⁵ C. S. Lindsey,³ C. Loomis,² J. M. LoSecco,⁵ T. McMahon,⁶ A. P. McManus,^{5,¶} N. K. Morgan,^{6,**} K. Nelson,^{7,¶} S. H. Oh,² N. T. Porile,⁶ D. Reeves,^{3,††} A. Rimai,⁶ W. R. Robertson,² R. P. Scharenberg,⁶ S. R. Stampke,^{5,‡‡} B. C. Stringfellow,⁶ M. A. Thompson,⁷ F. Turkot,³ W. D. Walker,² C. H. Wang,^{4,§§} J. Warchol,^{5,†} D. K. Wesson,^{2,|||} and Y. H. Zhan,^{5,¶¶}

¹Department of Physics, DePauw University, Greencastle, Indiana 46135

²Department of Physics, Duke University, Durham, North Carolina 27706

³Fermi National Accelerator Laboratory, P.O. Box 500, Batavia, Illinois 60510

⁴Department of Physics, Iowa State University, Ames, Iowa 50011

⁵Department of Physics, University of Notre Dame, Notre Dame, Indiana 46556

⁶Department of Physics and Chemistry, Purdue University, West Lafayette, Indiana 47907

⁷Department of Physics, University of Wisconsin, Madison, Wisconsin 53706

(Received 5 October 1992)

Experiment E735 collected data for $\sim 10^7$ interactions at the C0 intersection of the Fermilab $p\bar{p}$ collider with $\sqrt{s} = 1.8$ TeV. The Bose-Einstein correlations between pairs of identical pions were measured in a limited aperture spectrometer and used to estimate the size and lifetime of the source. The aperture shape limited the sensitivity primarily to the source dimension R along the incident $p\bar{p}$ direction. Both this dimension and the lifetime appear to depend strongly on pion multiplicity. Efforts were also made to obtain some information on the transverse source size, energy density, and the dependence of source size and strength on dipion momentum. Fits to the entire data sample yielded a value $R = 1.06 \pm 0.07$ fm for the average source dimension and a value $\tau = 0.74 \pm 0.06$ fm for the average source lifetime with $\langle dN_c/d\eta \rangle = 14.4$.

PACS number(s): 13.85.Ni, 12.40.Ee

I. INTRODUCTION

When two identical bosons are sufficiently close in phase space, one expects to see a probability enhancement due to Bose-Einstein symmetry. An early application of this effect was exploited by Hanbury Brown and Twiss [1] who used photon intensity interference to measure the size of astronomical sources.

These same ideas can be applied to identical pions provided the source collision contains enough energy to produce identical pion pairs. Goldhaber *et al.* [2] presented the first sample of data large enough to permit examination of the small part of phase where pion symmetry produced a significant effect. Later experiments at the CERN Intersection Storage Rings (ISR) proton collider [3–5] produced copious pions which made it possible to use the interference of identical pions as a tool for probing the spatial and temporal dimensions of the hadronic interaction region.

Application of the technique to a particular type of collision has usually been limited only by the number of pairs available for analysis. The enormous number of pions produced in high-energy heavy-ion collisions has allowed pion interferometry to become almost a routine procedure. Several reviews of pion interferometry with extensive references have been published by Zajc [6–8]. In what follows we present a study of pions produced in $p\bar{p}$ collisions at $\sqrt{s} = 1.8$ TeV.

II. MODELS

The physical interpretation of the data has been expedited by the use of two somewhat different models. The first, introduced by Kopylov and Podgoretsky [9],

*Now at University of Texas, Austin, TX 78712-1081.

†Now at Fermilab, Batavia, IL 60510.

‡Now at University of California, Riverside, CA 92521.

§Now at George Washington University, Washington, D.C. 20052.

||Now at University of Zurich, CH-8001 Zurich, Switzerland.

¶Now at University of Virginia, Charlottesville, VA 22901.

**Now at Virginia Polytechnic Institute, Blacksburg, VA 24061.

††Now at 9735 St. Augustine Rd., Jacksonville, FL 32257.

‡‡Now at SSCL, Dallas, TX 75237.

§§Now at Duke University, Durham, NC 22706.

|||Now at University of Massachusetts, Amherst, MA 01003.

¶¶Now at System Resources Consulting, Inc., Oakbrook, IL 60481.

considers pion emission to be from plane-wave sources distributed on the surface of a sphere of radius R . A symmetrized wave function is formed from two of these sources using Breit-Wigner denominators with an emission time τ . The square of the wave function is integrated over all energies and emission points in a way that makes the result analogous to optical radiation from a disk.

The integration leads to a natural set of momentum coordinates for the two-particle problem. $\mathbf{q} = \mathbf{p}_1 - \mathbf{p}_2$ is the momentum difference vector for the two pions as observed in the laboratory system. \mathbf{q}_t and \mathbf{q}_L are, respectively, the transverse and longitudinal components of \mathbf{q} with respect to $\mathbf{p} = \mathbf{p}_1 + \mathbf{p}_2$, the vector momentum of the two-pion system.

In terms of these variables the probability of observing two identical pions is [9]

$$C_2 = 1 + \left[\frac{2J_1(q_t R)}{q_t R} \right]^2 \left[\frac{1}{q_0^2 \tau^2 + 1} \right], \quad (1)$$

where the energy difference of the observed pions is $q_0 = E_1 - E_2$ [10], and J_1 is the first-order Bessel function.

In a continuing analogy with optics, if either the source or detector lacks symmetry about the observation axis, then \mathbf{q}_t has a preferred direction, and R is better interpreted as the conjugate source dimension parallel to the preferred direction of \mathbf{q}_t .

The second model simply assumes symmetrized free particle wave functions for the pions with Gaussian source-density weights $\rho(\mathbf{r})$ and $\rho(t)$ for the intensity. If

$$\rho(\mathbf{r})\rho(t) = \exp(-x^2/2x_0^2 - y^2/2y_0^2 - z^2/2z_0^2) \\ \times \exp(-t^2/2\tau^2),$$

then the Fourier transform of intensity for a spherical source yields the form to be expected for the two-pion correlation function [11]:

$$C_2 = 1 + e^{-|q|^2 R^2 - q_0^2 \tau^2}, \quad (2)$$

where $\mathbf{q} = \mathbf{p}_1 - \mathbf{p}_2$, and $q_0 = E_1 - E_2$. When $|q|^2$ is evaluated in the two-pion rest system, it assumes the value of the square of the invariant four-momentum difference $Q^2 = (p_1 - p_2)^2 = M_{2\pi}^2 - 4m_\pi^2$, where $M_{2\pi}$ is the mass of the two-pion system. In that case Eq. (2) becomes

$$C_2 = 1 + e^{-Q^2 R^2}. \quad (3)$$

The use of the invariant makes this an attractive model when trying to compare results from different types of experiments.

Numerous variations of these two models are possible. In comparing data one must be careful to specify the exact model used, since the parameters (R and τ) extracted from fits of the various models to the data can be systematically different by significant factors.

III. APPARATUS

The floor plan of the E735 apparatus is shown in Fig. 1. Various performance details of the individual com-

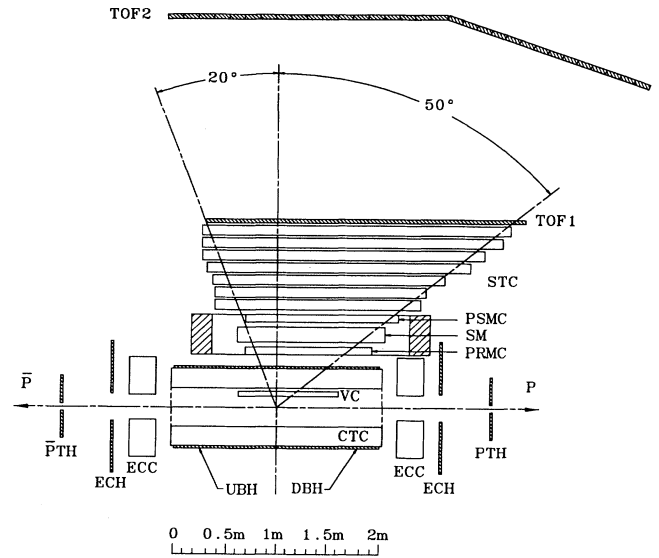


FIG. 1. Plan view of E735 detector. $\bar{\text{P}}\text{TH}$ = antiproton trigger hodoscope, ECH = end cap hodoscope, ECC = end cap chambers, UBH = upstream barrel hodoscope, DBH = downstream barrel hodoscope, PTH = proton trigger hodoscope, CTC = central tracking chamber, VC = vertex chamber, PRMC = premagnet chamber, SM = spectrometer magnet, PSMC = post magnet chamber, STC = straw tube chambers, TOF1 = time of flight No. 1 hodoscope, TOF2 = time of flight No. 2 hodoscope.

ponents have been reported elsewhere [12–18]. We will outline some of the essential features here.

A trigger was formed using hodoscopes with 15 scintillation counters each [proton trigger hodoscope (PTH), antiproton trigger hodoscope ($\bar{\text{P}}\text{TH}$)] located outside the beam pipe upstream and downstream of the collision point. The field free interaction region was surrounded by a 240 element hodoscope [end cap hodoscope (ECH), upstream barrel hodoscope (UBH), downstream barrel hodoscope (DBH)] which was complemented by drift chambers [charge tracking chamber (CTC), end cap chamber (ECC)].

A magnetic spectrometer viewed the beam crossing point on one side at $\theta \approx 90^\circ$ with respect to the colliding $p\bar{p}$ beams. Spectrometer tracking was provided by a vertex drift chamber (VC), two magnet drift chambers [pre-magnet chamber (PRMC), post magnet chamber (PSMC)], and a set of straw tube chambers (STC). The defining magnet aperture was roughly 1.20 rad along the beam direction and 0.35 rad orthogonal to the beam. Time-of-flight (TOF) scintillator planes 2.0 m and 4.0 m from the beam line provided simple mass discrimination for all particles with momenta up to 1.5 GeV/c. Mass discrimination was possible with reduced accuracy for some particles with momenta as high as 3.0 GeV/c.

The charged particle multiplicity N_h used in this report was measured using the 240 element hodoscope over a pseudorapidity range $|\eta| < 3.25$, where $\eta = \ln[\cot(\theta/2)]$, and θ is the polar track angle with respect to the incident proton direction. An estimate of

the true charged multiplicity N_c was obtained from N_h using tracking information in the spectrometer arm. The prescription for converting N_h to N_c is described in Ref. [12].

IV. DATA SELECTION

The experiment collected approximately 10^7 pions in the magnetic spectrometer. Raw data collected for this analysis consisted of $\sim 0.52 \times 10^6$ track pairs with both particles positively charged and $\sim 0.40 \times 10^6$ track pairs with both particles negatively charged. A Monte Carlo study found the difference between the number of positive and negative pairs is well explained by the acceptance aperture of the magnetic spectrometer.

Every event used in this analysis was required to have at least two hits each in the upstream and downstream trigger hodoscopes ($\bar{P}TH$ and PTH in Fig. 1). These counters lay outside the vacuum pipe and were essentially insensitive to all particles within 3.5 mrad of the beam line. This requirement discriminated heavily against beam-gas interactions, but because of it, double diffractive and single diffractive events were not collected efficiently.

Additional discrimination against beam-gas interactions was obtained by a cut on multiplicity asymmetry in the end cap hodoscopes (ECH in Fig. 1). A study of beam-gas scattering from single bunch stores of protons or antiprotons was used to determine a symmetric acceptance contour in the $(N_u - N_d)$ vs N_h plane, where N_u and N_d were, respectively, the number of hits for an event in the upstream and downstream hodoscopes, and N_h was the entire number of hodoscope hits for the event.

Average hit times were calculated separately for the upstream, downstream, and barrel hodoscopes (ECH, UBH, DBH). If any one of these averages deviated from the nominal beam crossing time by more than 6 nsec, the entire event was rejected from further analysis. This cut reduced beam-gas contamination as well as contributions to the data from interactions of satellite bunches. Lightly populated buckets of satellite particles commonly existed 19 nsec on either side of the primary bunch.

Except where noted, the full aperture of the magnet was used. This necessarily permits a small contamination by pions scattered or produced in the steel pole tips. We estimate that additional quality cuts described below removed these scattered particles from the analysis to a level of less than 1% of individual particles. In any case, such particles would not be expected to influence the measured source dimensions, but they might reduce the magnitude of the apparent two-particle correlation.

Pions with momentum less than 60 MeV/c could not reach the first TOF counter because of energy loss in the 2 mm aluminum beam pipe wall and subsequent spectrometer material. Tracks with momentum below 100 MeV/c appeared somewhat more susceptible to contamination by secondaries from beam-gas collisions and to charge-sensitive aperture effects, so that a decision was made to omit these from the analysis.

Tracks were not used in the analysis if the fit to the

chamber points had $\chi^2 > 8$. This was consistent with satisfactory performance by the tracking program for the spectrometer arm. Tracks for a pion pair were required to have projected origins at the beam separated by no more than 1 cm along the beam direction. (Two-track rms resolution was 3 mm.) Events having interaction vertices within 50 cm of the nominal center of the interaction region were accepted. The true interaction vertex distribution had a rms width of 30 cm.

Some of the tracking chambers and the TOF1 hodoscope inefficiently resolved track pairs with opening angles less than 10° in the x - z plane. By comparing to Monte Carlo generated tracks, we estimate that 25% of the pairs with opening angles less than 10° are lost in reconstruction. The final analysis uses no pion pairs with relative angles in the x - z plane less than 12° . This cut efficiently eliminates e^+e^- pairs, but not all electrons. Particle pairs used in the analysis contained $\sim 3\%$ of particles identified as electrons. In the interference region ($q_t < 0.2$), $\sim 5\%$ of the identified particles were electrons. There were no events containing identified electron pairs of the same sign.

V. MASS IDENTIFICATION

A simplified procedure was used to select a highly enriched sample of pion pairs without quite using the full ability of the TOF system to discriminate masses. Regardless of measured momentum, any track with an effective mass less than 400 MeV/c², as calculated by TOF1 or TOF2, was included in the analysis. Tracks without any successful mass identification, such as those which the magnetic field bent beyond the TOF1 plane, were arbitrarily assigned a pion mass.

Fewer than 20% of all tracks had no TOF mass identification. The multiplicity distributions of events with identified and unidentified tracks were essentially the same, although the unidentified tracks had a mean multiplicity 8% higher than those of identified tracks. Typically one expects 15% of these unidentified tracks to be nonpions, although at the higher momenta this may be as large as 45%. A track in the selected data sample thus has a 3–9% chance of not being a pion, and a track pair has a 0.1–0.8% chance of being a KK or pp pair. Pairs of nonidentical particles should have no effect on measurement of source sizes, but the measured correlation strength should appear to be reduced in proportion to their presence in the data sample.

The full set of selection criteria reduced the original data sample of 9.2×10^5 like-sign pairs to $\sim 1.5 \times 10^5$ $\pi^+\pi^+$ pairs and $\sim 1.1 \times 10^5$ $\pi^-\pi^-$ pairs.

VI. ACCEPTANCE EFFECTS

The two-pion relative momentum distributions of Eqs. (1) and (2) do not incorporate the multitude of experimental alterations of the data that must be present in real observations. The size of the problem is best illustrated by the experimental two-pion q_t distributions in Fig. 2(a). The absence of the simple constant term in Eqs. (1) and

(2) is perhaps the most remarkable feature of the distributions in Fig. 2. Also the distributions for $\pi^+\pi^+$, $\pi^-\pi^-$, and $\pi^+\pi^-$ are all different in a region where Bose-Einstein interference effects are to be studied. The depletion of events near $q_t=0$ is primarily due to vanishing phase space at zero relative momentum. The lack of events at larger q_t is mainly due to aperture restrictions on transverse momentum differences.

A similar set of distributions in Fig. 2(b) was generated by a Monte Carlo program using flat rapidity, flat azimuthal

angle, near-experimental p_t distributions, known spectrometer acceptance, and no Bose-Einstein symmetrization. The distributions in Fig. 2(b) are remarkably similar to the experimental distributions shown in Fig. 2(a) except for some small, important details at low q_t . These details are the result of Bose-Einstein symmetrization.

Since there is no possibility of observing an unbiased Bose-Einstein distribution experimentally, what must be obtained is the ratio of a Bose-Einstein distribution to a reference distribution that contains no Bose-Einstein symmetrization. For that ratio the constant term in Eqs. (1) and (2) describes the limit in the absence of any Bose-Einstein effect in both distributions. The value of 1.0 assumes the two distributions will be normalized to the same number of events in regions where the Bose-Einstein interference is inconsequential.

VII. REFERENCE DISTRIBUTIONS

One might consider obtaining an uncorrelated two-pion reference distribution from several sources: (1) Monte Carlo generated events, (2) $\pi^+\pi^-$ combinations using real data with both particles in the same event, or (3) $\pi^+\pi^+$ combinations using real data with each particle from a different event. The Monte Carlo method was not used because the required detail one needs to know about the detector and the production processes was prohibitive.

A Monte Carlo control experiment was performed to test the suitability of $\pi^+\pi^-$ pairs from the same event as an uncorrelated reference distribution. A sample of like-sign pion pairs and a sample of unlike-sign pion pairs were generated and tracked through the detector. The Monte Carlo events were subjected to the same cuts that were used on the experimental data. Neither sample contained Bose-Einstein effects. The ratio of like-sign/unlike-sign events is plotted in Fig. 3 as a function of q_t . The enhancement at low q_t is fit to a modified version of the Gaussian parametrization in Eq. (2): $C_2 = 1 + \lambda e^{-q_t^2 R^2}$. One obtains an apparent interaction radius of $R = 2.26$ fm and an apparent interference strength of $\lambda = 0.47$. The apparent radius is close to what is physically anticipated, and the interference strength is somewhat greater than that which we ultimately observe in this experiment.

The origin of this correlation is the different acceptance of the apparatus for π^+ and π^- mesons. Consequently we have not attempted to use $\pi^+\pi^-$ pairs as the reference distribution in this paper [19].

The reference distribution finally used was made by selecting and combining like-sign pion tracks from different events found in the real data sample. These tracks were subjected to experimental cuts that were identical to those for the like-sign pairs taken from the same event. In addition tracks from different events were required to share the same vertex location to within 1 cm and to have the same charged multiplicity N_h to within five particles.

For the purposes of further discussion the experimental correlation function was always calculated using

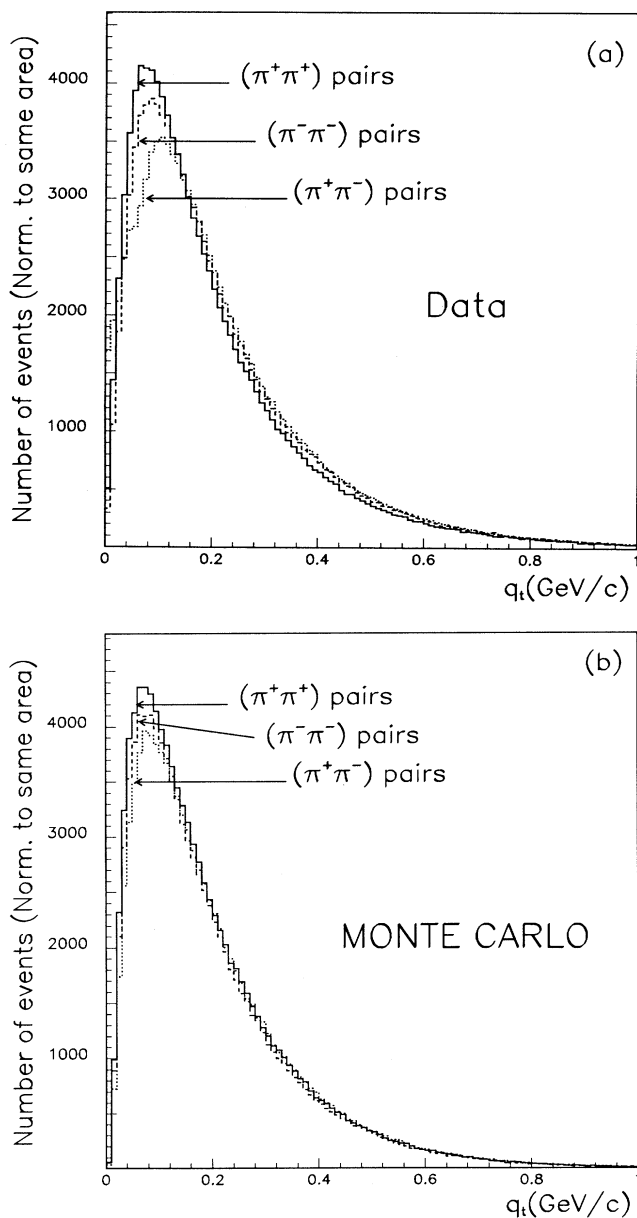


FIG. 2. (a) q_t distributions of pion pairs from real data. (b) q_t distributions of pion pairs from Monte Carlo events with no Bose-Einstein effects included. Distributions of different-sign combinations are normalized to the same area for comparison. These curves show the gross effects of experimental acceptance on pion pairs of different charge signs.

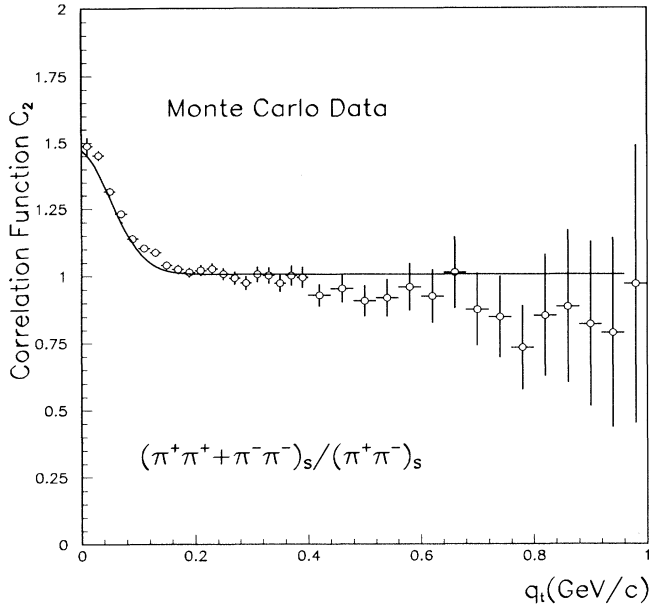


FIG. 3. Ratio of like-sign/unlike-sign pion pairs from Monte Carlo events that have no Bose-Einstein symmetry included in the event generation. Both numerator and denominator of the correlation function were formed using same-event pion pairs. The enhancement at small q_t is the result of the different experimental acceptance for π^+ and π^- .

$$C_2 = (\pi^+\pi^+ + \pi^-\pi^-)_S / (\pi^+\pi^+ + \pi^-\pi^-)_D,$$

where the denominator was the number of pion pairs at a point in a different-event reference distribution, and the numerator was the number at a corresponding point of a same-event distribution. Experimental correlation functions used in this paper were all computed with five times as many reference pairs in the denominator, appropriately renormalized, as same-event pairs in the numerator.

To avoid introducing artificial correlations, it was also necessary to ensure that the different-event reference pairs had the same vertex distribution along the beam line as same-event pairs. This does not occur naturally, since different-event track pairs normally have a vertex distribution that is the square of the same-event vertex distribution. The proper vertex distribution was achieved by generating the reference distribution twice. The second generator used an acceptance probability at each vertex position, determined from the first distribution, so as to yield the correct distribution of same-event vertex locations.

VIII. INTERACTION SIZE

Figure 4 shows the experimental two-pion correlation as a function of q_t for all pion pairs passing previously described cuts. Ideally one would choose events with $q_0=0$ to optimize the interference effect seen with respect to q_t . As a practical matter events with $q_0 < 0.200$ GeV were used in order to obtain a data sample of finite size. We will correct for this choice later in cases where it is necessary. Only track pairs with opening angles greater than 12° were used so as to avoid the inefficiencies in

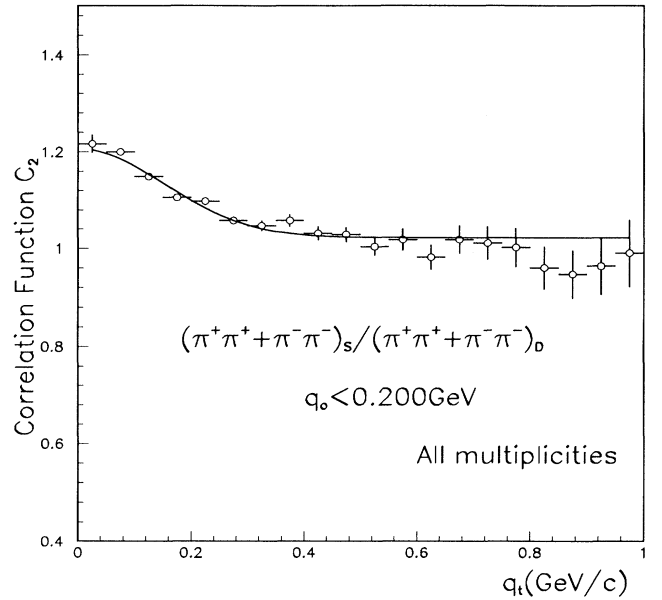


FIG. 4. Experimental ratio from the entire data sample of like-sign pion pairs from the same event to like-sign pion pairs from different events vs q_t . $\langle dN_c/d\eta \rangle = 14.4$ for these events.

tracking and particle identification mentioned earlier. Since no discernible difference could be detected between $\pi^+\pi^+$ and $\pi^-\pi^-$ distributions, they were combined in this plot [20].

The entire data sample was fit to the form $C_2 = 1 + \lambda e^{-\beta q_t^2}$, so that the constant λ contained the integrated dependence of q_0 and q_L appearing in Eq. (2). Prior to fitting, the number of pairs from same events (numerator of C_2) was normalized to the number from different events (denominator of C_2) for $q_t > 0.6$ GeV/c. The value obtained for the radius was $R = \hbar c \beta^{1/2} = 1.06 \pm 0.07$ fm. Because of the detector's restricted geometrical acceptance, this "radius" should be interpreted as predominantly a measure of interaction length along the beam (z) direction. Trigger restrictions for the entire data sample resulted in $\langle dN_c/d\eta \rangle = 14.4$, so that this value of R should be associated with that pseudorapidity density.

A distribution for C_2 similar to that above was obtained as a function of q_0 by restricting q_t such that $q_t < 0.200$ GeV/c. The fitted curve yielded a value of $\tau = 0.74 \pm 0.06$ fm for this average sample of data. One might interpret τ as the lifetime of the interaction as suggested by the Kopylov-Podgoretsky formulation or perhaps an interaction depth conjugate to q_L [10,21,22].

The number of pion pairs in the data was sufficient to support a limited investigation of source size as a function of charged multiplicity. Charged multiplicity, N_c , was determined using the scintillator hodoscope covering the pseudorapidity range $|\eta| < 3.25$. The full aperture of 4π steradians was expected to have a charged multiplicity about twice as large as N_c on the average. It should be noted that the acceptance aperture of the multiplicity hodoscope is more than an order of magnitude larger than that of the pion pair spectrometer.

Events were partitioned according to intervals of N_c . The same cuts and fitting procedures were used for these data intervals as those employed for the larger sample of data in Fig. 4. Representative plots as a function of q_t appear in Fig. 5 for three statistically independent intervals of multiplicity.

A summary of the fits to obtain source radius is shown in Fig. 6 as a function of pseudorapidity density $dN_c/d\eta$. One should realize that the selection of multiplicity intervals is such that adjacent intervals are not completely statistically independent. See details in Table I.

The value of $dN_c/d\eta$ is taken to be the ratio of $\langle N_c \rangle$ to the hodoscope pseudorapidity interval $\Delta\eta=6.5$, since the number of pions per unit η is essentially constant in this interval [23]. A significant increase of source size is seen to accompany increasing $dN_c/d\eta$.

All the plotted values of R in this paper were obtained by fitting to the same Gaussian parametrization. The radius R_G obtained from Gaussian fits is simply related to that obtained with fits to the Kopylov-Podgoretsky parametrization R_{KP} by $R_{KP} \simeq 2.0R_G$. Within statistics both parametrizations fit the data points equally well.

Also plotted in Fig. 6 are two data points from the Axial Field Spectrometer at ISR. These points combine $p\bar{p}$

and $p\bar{p}$ data for \sqrt{s} values at 63 and 53 GeV [4]. We have estimated $dN_c/d\eta$ for these points using accompanying charged multiplicity measured in the range $|\eta| < 1.0$. The points plotted are for pairs selected with the momentum difference \mathbf{q} preferentially aligned with a unit vector, $\hat{\mathbf{z}}$, along the beam axis such that $|\langle \mathbf{q} \cdot \hat{\mathbf{z}} \rangle / q| > 0.6$. This angular selection makes the data more comparable to the present experiment where $\langle |\langle \mathbf{q} \cdot \hat{\mathbf{z}} \rangle / q| \rangle = 0.767$. The ISR values of R_{KP} were divided by 2 to convert them to R_G for plotting in Fig. 6.

The UA1 data points in Fig. 6 are not as easily compared to those of the present experiment. They are from $p\bar{p}$ collisions with $\sqrt{s} \simeq 630$ GeV [24]. Particle pairs were accepted in a pseudorapidity interval $|\eta| < 3.0$ and an azimuthal interval of 150° . Since there is little restriction on the angle of \mathbf{q} with respect to the beam, these data points probably represent measurement of some average of the transverse and longitudinal source dimensions.

The correlation ratio $C_2 = 1 + \lambda e^{-aq_0^2}$ has been fit as well to the Gaussian parametrization for a range of multiplicities while continuing to constrain $q_t < 0.200$ GeV/c. Results are plotted in Fig. 7, where we have used the parameter $\tau = \hbar c \alpha^{1/2}$. At higher $dN_c/d\eta$, τ appears to approach a limiting value of ~ 1 fm. If τ is interpreted as a measure of transverse source size, it might be expected to increase with increasing overlap of the colliding hadron disks and perhaps saturate at the disk radius. Multiplicity might also be expected to increase with disk overlap.

Regardless of the limited azimuthal aperture of the spectrometer, an effort was made to obtain some more direct information on the transverse dimension of the source size. Equation (2) was reformulated in terms of transverse and longitudinal source sizes R_{xy} and R_z together with the corresponding components of \mathbf{q} :

$$C_2 = 1 + e^{-q_{xy}^2 R_{xy}^2 - q_z^2 R_z^2 - q_0^2 \tau^2}.$$

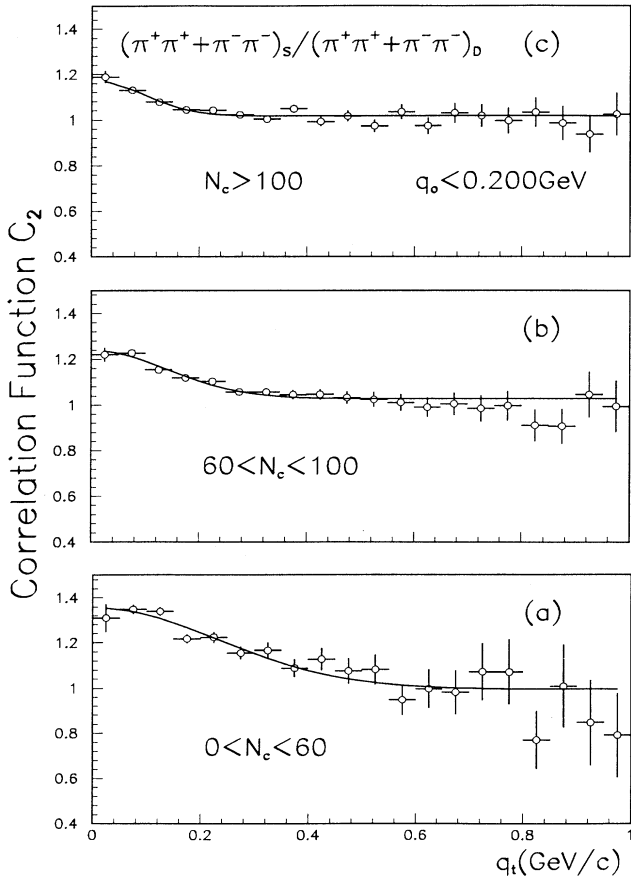


FIG. 5. Experimental correlation ratio C_2 vs q_t using events with charged multiplicity (a) $N_c < 60$, (b) $60 < N_c < 100$, and (c) $N_c > 100$.

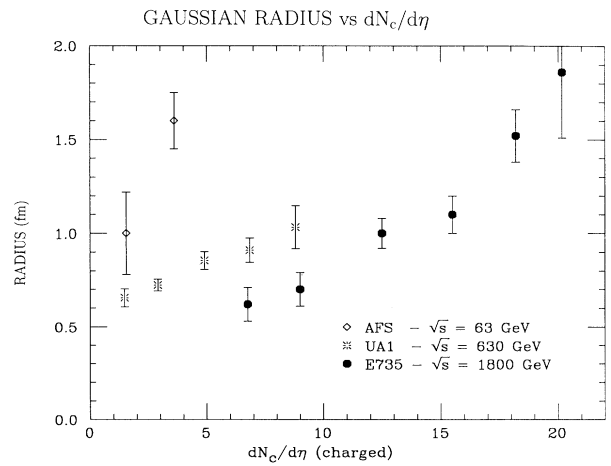


FIG. 6. Interaction “radius” vs $dN_c/d\eta$, charged particle multiplicity per unit of pseudorapidity. Experimental conditions for ISR [4] and UA1 [24] points differ from those of E735 in a number of respects. Adjacent points from the present experiment are not statistically independent. See tabular data for details.

TABLE I. Fitted values of radius R_G , lifetime τ , and corrected chaoticity λ in the Gaussian parametrization with respect to q_t and q_0 . Values are a function of average charged multiplicity per unit of pseudorapidity. Charged multiplicity intervals containing the data are listed in column 1. The errors are statistical.

N_c	$\langle dN_c/d\eta \rangle$	R_G (fm)	τ (fm)	λ
0–60	6.75	0.62 ± 0.09	0.53 ± 0.07	0.39 ± 0.05
0–80	9.00	0.70 ± 0.09	0.65 ± 0.06	0.32 ± 0.03
60–100	12.5	1.00 ± 0.08	0.86 ± 0.12	0.25 ± 0.01
80–120	15.5	1.10 ± 0.10	0.89 ± 0.12	0.23 ± 0.01
100–240	18.2	1.52 ± 0.14	0.99 ± 0.15	0.21 ± 0.02
120–240	20.17	1.86 ± 0.35	0.88 ± 0.20	0.19 ± 0.03

It was just possible to obtain enough statistics in order to fit the form $C_2 = 1 + \lambda e^{-q_{xy}^2 R_{xy}^2}$ by using the entire sample of data. Values of q_0 and q_z were constrained to be less than 0.200 GeV in the same manner as in previous fitting.

The fit value for the transverse dimension was $R_{xy} = 0.73 \pm 0.05$ fm. A similar procedure for the longitudinal dimension gave $R_z = 0.89 \pm 0.04$ fm. R_z is somewhat smaller than the value R_G obtained from the entire data sample, indicating a systematic difference between use of the variables q_z and q_t .

Finally, a radius was obtained by fitting data plotted with respect to the invariant Q with the form $C_2 = 1 + \lambda e^{-\gamma Q^2}$. In this case $R_Q = \hbar c \gamma^{1/2}$. For our sample of data, we find from comparing plots of R_Q and R_G vs multiplicity that R_Q is simply related to the Gaussian radius R_G with respect to q_t by $R_Q \simeq 0.254 + 1.023 R_G$ when radii are expressed in femtometers. Some potential information may be obscured by the use of this single parameter to describe the data. A tabulation of these fit parameters appears in Table II. It should be noted that for the higher pair momenta of this experiment Q^2 reduces approximately to q_t^2 . For that range of the data $R_Q \simeq R_G$.

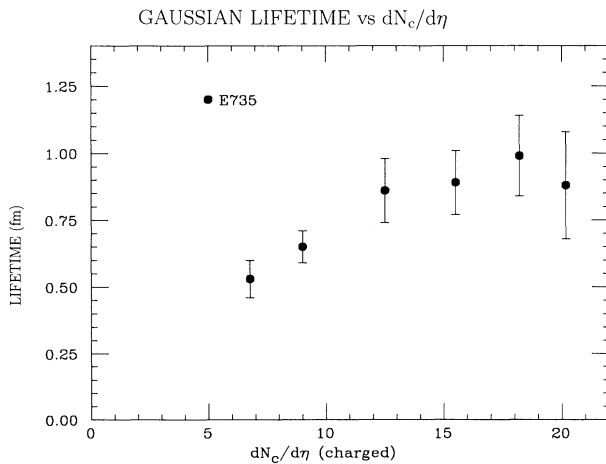


FIG. 7. Fit parameter τ conjugate to q_0 as a function of $dN_c/d\eta$, charged particle multiplicity per unit of pseudorapidity.

IX. CHAOTICITY

When the interference region is fit to $C_2 = 1 + \lambda e^{-\beta q_t^2}$, one obtains a value for the parameter λ which is less than the maximum theoretical value of $\lambda = 1.0$. The value of λ should presumably be 1.0 when the production phases of the two particles are completely random, since intensity interference experiments such as this one depend on an average over phases [25]. A completely coherent source could conspire to produce no enhancement in the low q_t region. The parameter λ is sometimes called the “coherence parameter” [8] or the “chaoticity” [26].

Figure 8 is a plot of λ as a function of $dN_c/d\eta$ for fits with respect to the variable q_t . For our restricted aperture the value of λ decreases with increasing multiplicity. The relative number of phase-correlated pion pairs in our acceptance appears to increase with multiplicity.

Because the widths of the q_t and q_0 distributions both change with increasing multiplicity, it is necessary to correct the fitted λ values. Previous fits to either variable were made with events that allowed the other variable to range from 0 to 0.200 GeV, the same q_t (or q_0) interval in which the widths were changing most.

The effect of the changing widths on the strength of the interference was studied using a Monte Carlo program to generate the Bose-Einstein events with a known $\lambda = 0.5$, $R = 1.0$ fm, and $\tau = 0.7$ fm. Applying the experimental cuts to the Monte Carlo events and fitting the resulting distributions gave an estimate of the corrections needed for λ . Figure 8 plots the corrected λ appropriate for use in the equation $C_2 = 1 + \lambda e^{-|q|^2 R^2 - q_0^2 \tau^2}$. The result was that values of R and τ found earlier required no correction for this effect. On the other hand, values of λ

TABLE II. Fitted values of radius R_Q and chaoticity λ using a Gaussian distribution in the invariant parameter Q . Quoted errors are statistical.

N_c	$\langle dN_c/d\eta \rangle$	R_Q (fm)	λ
0–60	6.75	0.86 ± 0.04	0.40 ± 0.02
0–80	9.00	1.02 ± 0.05	0.27 ± 0.02
60–100	12.5	1.26 ± 0.05	0.24 ± 0.02
80–120	15.5	1.46 ± 0.10	0.24 ± 0.02
100–240	18.2	1.70 ± 0.12	0.23 ± 0.02
120–240	20.17	2.46 ± 0.32	0.20 ± 0.04

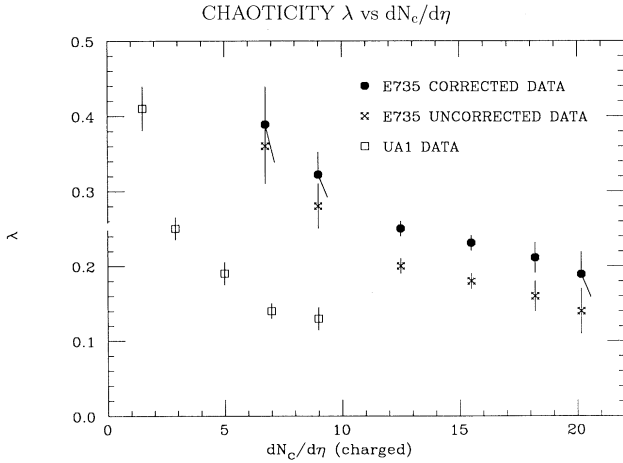


FIG. 8. Chaoticity factor λ as a function of pseudorapidity density of charged particles, $dN_c/d\eta$. The UA1 data point at lower values of $dN_c/d\eta$ were taken from Ref. [24].

had to be systematically increased. After corrections the λ values from q_0 fits were in agreement with those from q_t fits as one would expect. The corrected values of λ are presented in Table I.

When the correlation function $C_2 = 1 + \lambda e^{-rQ^2}$ was fit as a function of the single invariant Q^2 , no correction was necessary for the chaoticity factor. Values of λ were essentially the same within errors as the corrected ones using q_t fits. Data for these fits are presented in Table II.

Also plotted in Fig. 8 are values of λ measured by UA1. These values were obtained at lower energies ($\sqrt{s} \approx 630$ GeV), and no particle identification was used to choose pion pairs [24]. Using particle ratios measured in our experiment, one might expect 30–40% of their pairs would contain at least one proton, kaon, or lepton. The presence of these contaminated pairs would reduce the effective λ .

As mentioned in the discussion of interaction size, the selected pairs in the UA1 experiment were much less restricted by geometry than in the present experiment. We are unable to determine the relative importance of the energy and geometry in producing the differences seen between the two experiments in Fig. 8. However, the net result is that the present experiment observes an interference effect which is several times stronger than that observed by UA1.

X. COHERENT SOURCES

The values of λ for pions produced in e^+e^- experiments are typically about two times larger than those for pions produced in hadron collisions. After removing pions which can be associated with resonance decay, some e^+e^- experiments report values of λ compatible with $\lambda = 1.0$ [27,28].

The theoretical effect of including one pion from a resonance decay in the pion pair has been studied by Bowler [29]. He finds that in principle the presence of resonance decays can reduce the measured size of λ significantly.

Monte Carlo calculations with PYTHIA [30] indicate that we should expect about 80% of the pions in this experiment to be secondary pions from resonance decay rather than primary pions. With such a large number of secondary pions, only $\sim 4\%$ of the pion pairs accepted by the spectrometer aperture would consist of two primary pions.

We have attempted an experimental study of some resonances which have finite acceptance in our small spectrometer aperture. These are K^* , K_S^0 , Λ , ρ , $\omega + \eta$, Ξ , Ω , and ϕ . Preliminary calculations in this study are in agreement with the possibility that more than 50% of our observed pions come from resonance decays.

XI. MOMENTUM DEPENDENCE

The observed interaction radius does exhibit a dependence on the momentum of the pion pair. It becomes increasingly difficult to measure the radius at lower pair momenta where we have accumulated very few pairs with q_t values larger than the enhancement region. Therefore normalization of the reference sample to the interference data cannot be done as reliably outside the enhancement region. Some systematic error may come about because of this, but it would appear to be substantially smaller ($< 20\%$) than the observed variation of radius with pair momentum.

Figure 9 shows the Gaussian source radius as a function of pair momentum, $P_{\pi\pi}$. Since the spectrometer arm is predominantly perpendicular to the beam ($45^\circ < \theta < 100^\circ$), pair momentum is essentially transverse momentum. See Table III for corresponding p_T values.

The radius parameter R does not depend as strongly on pair momentum as it does on event multiplicity. Low momentum and high multiplicity both lead to a larger radius. A similar increase in the value of τ is seen as the momentum decreases, but the chaoticity λ has no significant dependence on pair momentum.

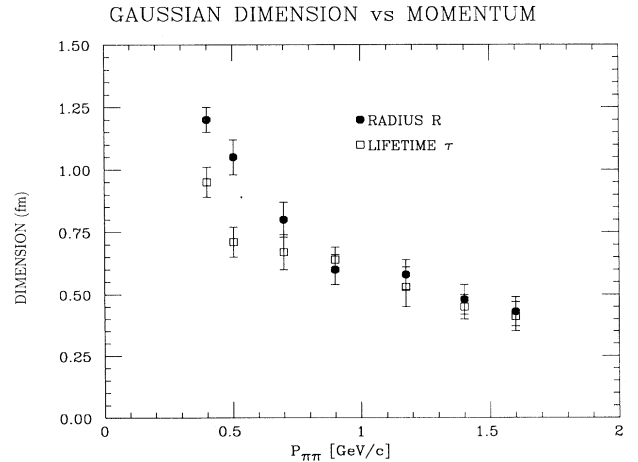


FIG. 9. Interaction “radius” and lifetime as a function of the total momentum $P_{\pi\pi}$ of the pion pair. R_G is primarily a source dimension along the beam direction. τ might possibly be interpreted as a source dimension transverse to the beam. Data are from Table III.

TABLE III. Fitted values of radius R_G , lifetime τ , and chaoticity λ in the Gaussian parametrization with respect to q_t and q_0 . Values are a function of average two-pion total momentum $P_{\pi\pi}$, or average two-pion transverse momentum P_T . The total momentum interval containing the data is listed in column 1. Momentum is in GeV/c. The errors are statistical.

$P_{\pi\pi}$	$\langle P_{\pi\pi} \rangle$	R_G (fm)	τ (fm)	λ	$\langle p_T \rangle$
0.2–0.5	0.404	1.20 ± 0.05	0.95 ± 0.06	0.24 ± 0.01	0.369
0.2–0.7	0.503	1.05 ± 0.08	0.71 ± 0.05	0.25 ± 0.01	0.462
0.5–1.0	0.708	0.80 ± 0.07	0.67 ± 0.07	0.23 ± 0.02	0.650
0.7–1.2	0.900	0.60 ± 0.06	0.64 ± 0.05	0.26 ± 0.03	0.832
0.9–1.7	1.175	0.58 ± 0.06	0.53 ± 0.07	0.26 ± 0.02	1.087
> 1.0	1.403	0.48 ± 0.06	0.45 ± 0.05	0.21 ± 0.02	1.285
> 1.2	1.600	0.43 ± 0.06	0.41 ± 0.06	0.23 ± 0.02	1.479

As pair momentum increases, the spectrometer acceptance might be expected to accommodate more pairs with q_t transverse to the beam line. If a large number of such pairs enters the data sample, the measured source size will become an average of the transverse and longitudinal dimensions. This might appear as decreasing source size with increasing pair momentum. We have checked the data for evidence of such an effect in the following way.

As a function of pair momentum we have investigated the relative amounts of data from four different orientations of q_t with respect to the beam axis: 0° – 15° , 15° – 30° , 30° – 45° , 45° – 60° . Although 60% of the data is in the first angular interval, the relative amount from each interval remains constant as a function of pair momentum. There is no disproportionate increase of pairs with q_t not parallel to the beam line as described above. It therefore seems that the longitudinal source size does indeed depend upon pair momentum and that the observed dependence on momentum is not simply an aperture effect. Unfortunately the data sample is not large enough to make a significant determination of source size as a function of the orientation of q_t .

XII. EXPANDING SHELL

Pratt [31,32] has suggested that pions might be emitted from an expanding spherical shell, where the outward shell velocity is v_t . In that case one would expect our experiment to measure a decreasing source size R with increasing pair momentum. The effect is qualitatively explained if one notes that pions observed at 90° with respect to the beam could get a momentum boost from the shell velocity if they were emitted close together, but could receive no boost if they were emitted at extreme separations along the beam direction.

The expression developed by Pratt for Bose-Einstein interference [31] is a function of R and $\gamma v_t/T$, where T is the temperature of the pions in the rest system of the shell, and $\gamma = 1/\sqrt{1-v_t^2}$. For a fixed value of T , we find our data exhibit a sensitivity to the ratio R/v_t , but are incapable of determining the values of R and v_t separately.

To investigate the general behavior to be expected for R with an expanding shell, we have fixed $T=140$ MeV and $v_t=1/\sqrt{3}$, the velocity of sound in a massless gas [33]. Some evidence for values of this order has been found from a study of particle momentum spectra [34].

Using these fixed parameters, we find the shell radius $R_S \simeq 2.0R_G$. Fits to our data show that the value of R_S increases with multiplicity and decreases with pair momentum in a fashion similar to the behavior of R_G . A more meaningful investigation of this model would require independent determinations of T and v_t .

XIII. CORRECTIONS

Zajc [7] has quantitatively described an extraneous correlation which can be introduced by experimental acceptance. The single-pion reference distributions from different events contain some particles which were members of correlated Bose-Einstein pairs. The effect on C_2 of including these particles in the reference distribution depends on the experimental aperture. Using a Monte Carlo program to generate both Bose-Einstein events and uncorrelated pions, we have estimated that $C_2 \simeq 1.07C_2^{\text{observed}}$. Our normalization of the like-sign pairs to the reference sample probably obscured this effect, so no correction for it has been attempted.

Like-sign pions in the same event can experience a Coulomb repulsion which is not the case for the like-sign pions from different events. In principle this can produce a correlation in C_2 due to the difference in the numerator and denominator. The Gamow correction factor G_l for Coulomb repulsion of like-sign charges [28,35] is explicitly a function of the invariant Q^2 and not q_t . The size of the effect for our data was estimated using Monte Carlo events weighted by G_l and plotted vs q_t . Comparison of fits to weighted and unweighted Monte Carlo events indicates that values of R , τ , and λ previously presented could be increased at most by about 2% because of Coulomb effects.

Since the radius is determined by measuring the enhancement width at small q_t , a random momentum measuring error which causes larger widths in q_t yields underestimates of the radius. We have studied the momentum resolution through its effect on the π , K , and p mass resolution and checked the result against the $K^0 \rightarrow 2\pi$ mass resolution. A good description of the momentum resolution averaged over the above studies is $\delta p/p = 4\% \sqrt{p^2 + 1/\beta^2}$, where p is in GeV/c. Using this error function, we have generated correlated Bose-Einstein pairs with a known radius. The estimated errors in q_t and q_0 were approximately 20 MeV. Figure 10

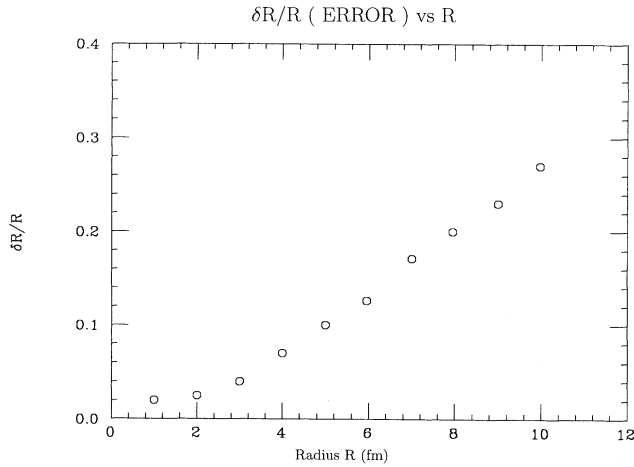


FIG. 10. Fractional error in interaction radius resulting from momentum measuring error as a function of the true radius. The measured radius is systematically smaller than the true radius. The relevant range of R for this experiment is $0.0 < R < 2.0$.

shows the fractional error in radius as a function of the known radius. Values of the interaction radius quoted in this paper are too small by about 2% because of imperfect momentum resolution.

XIV. SYSTEMATIC CHECKS

To provide reassurance that the enhancements we have measured are not the result of some systematic analysis error, we have applied our analysis to two sets of particle pairs that should not exhibit a symmetry enhancement. The same procedures and data cuts were used as previously for pion pairs.

The first set uses like-sign particle pairs with both particles mass identified to be unlike particles. Like-sign pairs of πK , pK , and $p\pi$ were used in calculating C_2 for both the same-event and different-event pair combinations. Regardless of mass identification, each track was assigned a pion mass in the analysis. A q_t distribution for this analysis appears in Fig. 11. No systematic enhancement is obvious.

The second set uses pion pairs of unlike sign in both the same-event and different-event combinations. This analysis could have some susceptibility to correlations induced by common resonance decay. Adequate statistics made it possible to search for correlations as a function of event multiplicity. A sample plot in Fig. 12 shows C_2 as a function of q_t for $60 < N_c < 100$. None of the plots contained a significant correlation. To some extent this may be due to the small acceptance of our aperture for pairs from resonance decay.

XV. ENERGY DENSITY

A measured increase of R and τ with increasing multiplicity suggests that, for those particles which yield this measurement, some related interaction volume increases with multiplicity. The implications of a volume which increases with multiplicity can be seen if one makes *any*

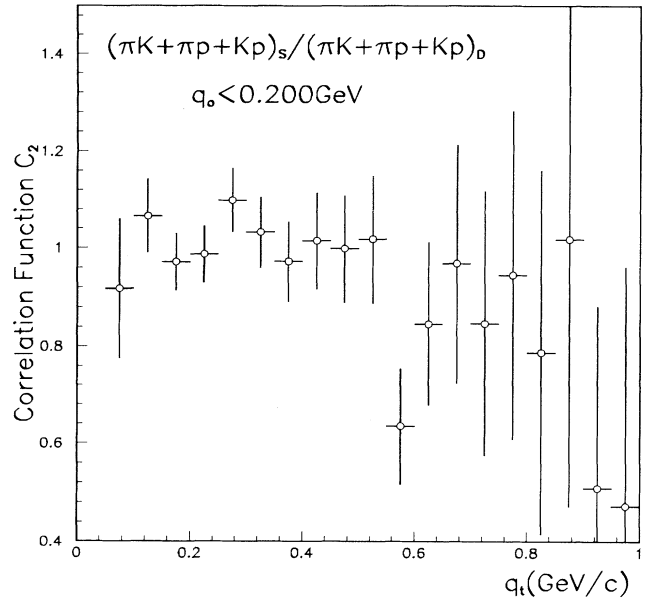


FIG. 11. Correlation function C_2 for like-sign particle pairs of $K^\pm \pi^\pm$, $p^\pm \pi^\pm$, and $p^\pm K^\pm$.

estimate of the energy density of the interaction. The first estimate we make here is perhaps a lower limit on energy density since it makes use only of the pions that contributed to a measurement of the source size parameters. As a calculational example we have chosen to use the parameters R_G and τ obtained from the Gaussian fits in the variables q_0 and q_t . These are listed in Table I.

Figure 13 contains a plot of this estimated energy density. The average number of pions $\langle N \rangle$ emanating from a measured interaction volume is taken to be

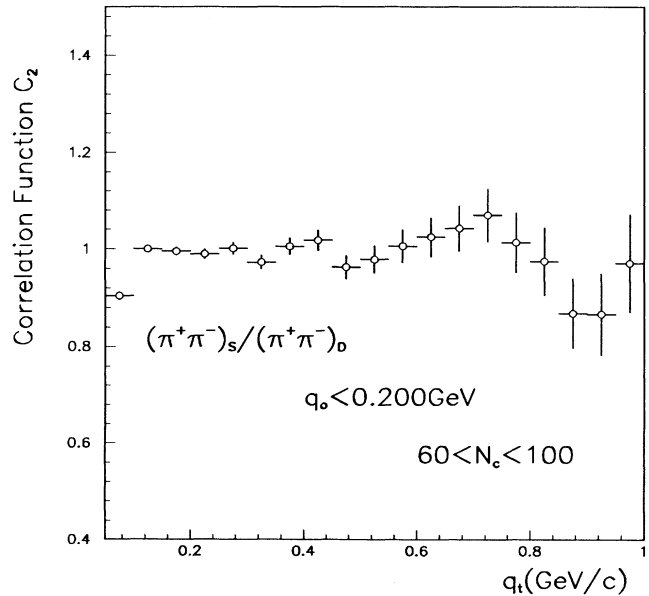


FIG. 12. Correlation function C_2 for unlike-sign pion pairs as a function of q_t . The sample plot shown is for event charged multiplicity $60 < N_c < 100$.

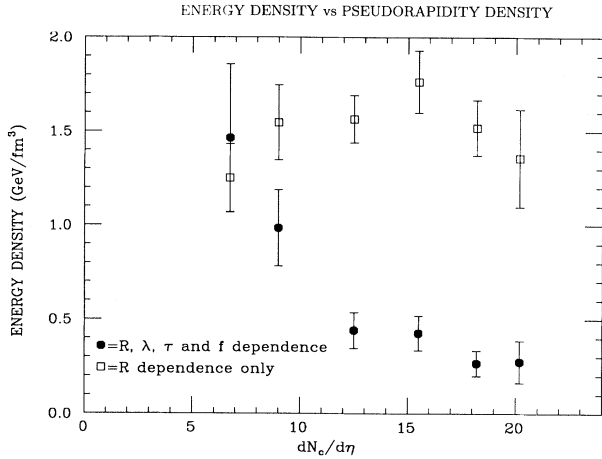


FIG. 13. Solid circles are estimates of the “chaotic” energy density in the interaction volume based on the multiplicity dependence of $\langle p_T \rangle$, λ , R , τ , and $\langle dN_c/d\eta \rangle$. Open squares are estimates of energy density including only the dependence of R on multiplicity.

$$\langle N \rangle = \frac{3}{2} \lambda f \langle dN_c/d\eta \rangle \Delta\eta_{\text{spec}}. \quad (4)$$

The factor $\frac{3}{2}$ is a correction for missing neutral pions. Chaoticity λ is used to allow for the fact that only a fraction of the pions is known to come from the measured volume. The other noninterfering pions, for example, may come from a volume of entirely different size. Pions that produced the size measurement were observed only in the spectrometer pseudorapidity interval $\Delta\eta_{\text{spec}} = 1.37$. The fraction f of charged particles which is composed of pions at a given rapidity is computed from the K/π and p/π ratios in Ref. [13] and is approximately $f \approx 0.84$.

Energy density ϵ is calculated in a spirit similar to that of Bjorken [36] who associates an energy deposition p_T with each observed particle. We assume each particle receives a collision energy equal to $\langle p_T \rangle$ measured for the relevant multiplicity [13]. A typical value is $\langle p_T \rangle \approx 0.38$ GeV/c. The volume is taken to be a cylinder with transverse radius τ and longitudinal dimension $2R$:

$$\epsilon = \langle N \rangle \langle p_T \rangle / 2\pi\tau^2 R. \quad (5)$$

The error bars shown in Fig. 13 are calculated statistically assuming errors in λ , τ , and R are uncorrelated.

Energy densities much larger than those calculated above can be obtained by assuming that other particles also originated in the measured volume. Using Eq. (4), one calculates that 4.6 pions originated in the volume for the point plotted at the lowest $dN_c/d\eta$. For the same $dN_c/d\eta$ the total number of particles, charged plus neutral, observed in 6.5 units of pseudorapidity was 65.8. Using these values instead would make the point at the leftmost pseudorapidity density of Fig. 13 an order of magnitude higher in energy density [37].

An alternative calculation of the energy density is one which omits the dependence of λ and τ on the multiplicity. In that case the increase in the cylinder volume with its length R is compensated for by an increase in multi-

city, so that the energy density is approximately constant with increasing multiplicity. These points for energy density are also plotted in Fig. 13, where the cylinder radius is assumed fixed at $\tau = 1.0$ fm and $\langle N \rangle = \frac{3}{2} \langle dN_c/d\eta \rangle \Delta\eta_{\text{spec}}$. Using the data presented in this paper, there is no combination of parameters which will produce an energy density that increases with multiplicity. This does not necessarily rule out those models which have such an increase at early times in the collision process.

One reason that there are no data points at lower multiplicity is that the lower multiplicity triggers were pre-scaled in favor of the higher multiplicity events by more than an order of magnitude. The experiment was designed to study these higher multiplicity events. In addition to this, lower multiplicity events simply have a smaller probability of producing pairs in a small aperture spectrometer.

XVI. MULTIPLICITY vs SIZE

Bjorken has suggested that hadronization might take place on the surface of some suitably defined interaction volume [38]. Particle multiplicity would then be proportional to the surface area rather than the volume.

To study this possibility, we have defined an area using the measured pion interference parameters to be that of a cylinder with $A = 2(\pi\tau^2 + 2\pi\tau R)$. Figure 14 shows the dependence on A of the average charged multiplicity $\langle N_c \rangle$ for $|\eta| < 3.25$. Values of $\langle N_c \rangle / 10$ have been plotted to facilitate comparison with the pion multiplicity $\langle N \rangle$ calculated in Eq. (4).

The total charged multiplicity N_c is clearly correlated with the area A with $A \approx 0.20 \langle N_c \rangle - 4.1$. Multiplicity N of the interfering pions is not as strongly related to the area with $A \approx 7.8 \langle N \rangle - 31$.

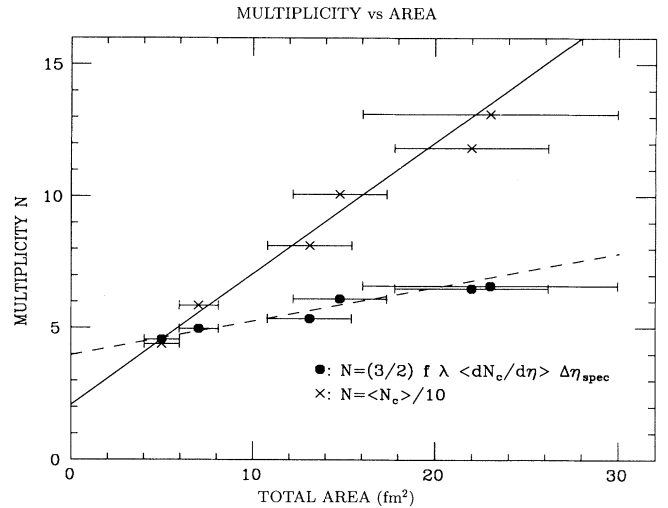


FIG. 14. Multiplicity vs area of the interaction volume. Crosses are for average charged multiplicity $\langle N_c \rangle / 10$ of all particles in the pseudorapidity interval $|\eta| < 3.25$. Circles are for charged-plus-neutral multiplicity of pions in the rapidity interval of the spectrometer, corrected downward by the chaoticity factor λ .

Similar plots can be made to exhibit the multiplicity dependence on volume, where the cylinder volume V is defined to be $V=2\pi\tau^2R$. For this case $V\simeq 0.084\langle N_c \rangle - 2.75$ and $V\simeq 3.2\langle N \rangle - 13.7$. Linear fits relating multiplicity to either volume or area appear to be equally appropriate within the experimental errors.

XVII. SUMMARY

The Bose-Einstein interference of pion pairs has been used to study interaction size of $p\bar{p}$ collisions at $\sqrt{s}=1.8$ TeV. The dimension R observed along the beam direction grows rapidly with the pseudorapidity density of produced particles.

The dimension τ complementary to energy difference or longitudinal momentum difference also grows with multiplicity. It tends to experience a growth saturation at higher multiplicity. To the extent that this variable can be interpreted as the depth of the interaction, it is a measure of the transverse source size [10,21,22].

The strength of the interference effect λ is the same when determined by fits either for R or τ . Its decrease with increasing particle multiplicity may imply the appearance of a source of phase-coherent pion pairs.

Both R and τ decrease with increasing momentum for the pion pair. This size variation is not as large as that due to multiplicity. The strength of the interference λ does not depend measurably on pion pair momentum. Such dependence on pair momentum is consistent with an expanding shell model as proposed by Pratt.

Using the size parameters measured in this experiment, we have made several estimates of energy density. These estimates show that energy density either decreases or at most remains constant with increasing $dN_c/d\eta$.

ACKNOWLEDGMENTS

We would like to thank J. D. Bjorken for continuing encouragement and advice. Discussions with Scott Pratt have been most useful and enlightening.

-
- [1] R. Hanbury Brown and R. Q. Twiss, *Philos. Mag.* **45**, 663 (1954).
 - [2] G. Goldhaber *et al.*, *Phys. Rev.* **120**, 300 (1960).
 - [3] M. Deutschmann *et al.*, *Nucl. Phys.* **B204**, 333 (1982).
 - [4] T. Akesson *et al.*, *Phys. Lett B* **187**, 420 (1987).
 - [5] T. Akesson *et al.*, *Z. Phys. C* **36**, 517 (1987).
 - [6] W. A. Zajc *et al.*, *Phys. Rev. C* **29**, 2173 (1984).
 - [7] W. A. Zajc, *Phys. Rev. D* **35**, 3396 (1987).
 - [8] W. A. Zajc, in *Hadronic Multiparticle Production*, edited by P. Carruthers (World Scientific, Singapore, 1988), p. 235.
 - [9] G. I. Kopylov and M. I. Podgoretsky, *Yad. Fiz.* **15**, 392 (1972) [*Sov. J. Nucl. Phys.* **15**, 219 (1972)].
 - [10] Since $q_0=0$ in the $\pi\pi$ rest system, in any other system we have that $q_0=\beta_{\pi\pi}q_L$, where $\beta_{\pi\pi}$ is the velocity of the $\pi\pi$ system. $q_0\simeq q_L$ for the data sample in this experiment.
 - [11] S. Y. Fung *et al.*, *Phys. Rev. Lett.* **41**, 1592 (1978).
 - [12] T. Alexopoulos *et al.*, *Phys. Rev. Lett.* **60**, 1622 (1988).
 - [13] T. Alexopoulos *et al.*, *Phys. Rev. Lett.* **64**, 991 (1990).
 - [14] T. Alexopoulos *et al.*, *Phys. Scr.* **T32**, 122 (1990).
 - [15] E. W. Anderson *et al.*, *Nucl. Instrum. Methods A* **295**, 86 (1990).
 - [16] S. Banerjee *et al.*, *Nucl. Instrum. Methods A* **269**, 121 (1990).
 - [17] T. Alexopoulos *et al.*, *Nucl. Instrum. Methods A* **311**, 156 (1992).
 - [18] C. Allen *et al.*, *Nucl. Instrum. Methods A* **264**, 108 (1990).
 - [19] Applying appropriate geometrical corrections to the experimental data, one can avoid this artificial correlation which is produced by using same-event $\pi^+\pi^-$ pairs as a reference distribution. Peter Beery, Ph.D. thesis, University of Notre Dame, 1990.
 - [20] T. Alexopoulos, Ph.D. thesis, University of Wisconsin, Madison, 1991.
 - [21] E. V. Shuryak, *Phys. Lett.* **44B**, 387 (1973).
 - [22] G. Cocconi, *Phys. Lett.* **49B**, 459 (1974).
 - [23] Chi-Ho Wang, Ph.D. thesis, Iowa State University, 1991.
 - [24] UA1 Collaboration, J. D. Dowell, in *Proceedings of the VIIth Topical Workshop on Proton-Antiproton Physics*, Batavia, Illinois, 1988, edited by R. Raja, A. Tollestrup, and J. Yoh (World Scientific; Singapore, 1988), p. 115; in *Proceedings of the XXIVth International Conference on High Energy Physics*, Munich, West Germany, 1988, edited by R. Kotthaus and J. Kuhn (Springer, Berlin, 1988); C. Albajar *et al.*, *Phys. Lett. B* **226**, 410 (1989).
 - [25] Gordon Baym, *Lectures on Quantum Mechanics* (Benjamin, New York, 1969), p. 431.
 - [26] R. M. Weiner, *Phys. Lett. B* **232**, 278 (1989).
 - [27] P. D. Acton *et al.*, *Phys. Lett. B* **267**, 143 (1991).
 - [28] I. Juricic *et al.*, *Phys. Rev. D* **39**, 1 (1989).
 - [29] M. G. Bowler, *Phys. Lett. B* **231**, 203 (1989); *Z. Phys. C* **46**, 305 (1990).
 - [30] T. Sjostrand and M. Zijl, *Phys. Rev. D* **36**, 2019 (1987).
 - [31] Scott Pratt, *Phys. Rev. Lett.* **53**, 1219 (1984).
 - [32] Scott Pratt, *Phys. Rev. D* **33**, 1314 (1985).
 - [33] S. R. de Groot and W. A. Vanleeuwen, *Relativistic Kinetic Theory* (North-Holland, Amsterdam, 1980), p. 256.
 - [34] P. Levai and B. Muller, *Phys. Rev. Lett.* **67**, 1519 (1991).
 - [35] A. S. Davydov, in *Quantum Mechanics*, edited by D. ter Haar (Pergamon, London, 1965).
 - [36] J. D. Bjorken, *Phys. Rev. D* **27**, 140 (1983). It should be noted that there is a difference in the definition of energy density used by Bjorken and that used in this paper. Bjorken considers the initial energy density of the thermalized partons, while in this paper we consider the energy density of only those pions giving rise to the measured correlations.
 - [37] In Ref. [12] the E735 Collaboration used Bjorken's formula in Ref. [36] to estimate the highest energy density to be $\epsilon\simeq 4$ GeV/fm³ at $dN_c/d\eta=32$.
 - [38] J. D. Bjorken (private communication).